ARTICLE

# Power and carbon monoxide co-production by a proton-conducting solid oxide fuel cell with $La_{0.6}Sr_{0.2}Cr_{0.85}Ni_{0.15}O_{3-\delta}$ for on-cell dry reforming of $CH_4$ by $CO_2$

Received 00th January 20xx,
Accepted 00th January 20xx

DOI: 10.1039/x0xx00000x

Tong Wei[‡a], Peng Qiu[‡a, b], Lichao Jia[a*], Yuan Tan[c], Xin Yang[b], Shichen Sun[b], Fanglin Chen[b*] and Jian Li[a]

To directly use $CO_2$-$CH_4$ mixture gas for power and CO co-production by proton-conducting solid oxide fuel cells (H-SOFC), a layer of in situ reduced $La_{0.6}Sr_{0.2}Cr_{0.85}Ni_{0.15}O_{3-\delta}$ (LSCrN@Ni) is fabricated on a Ni-$BaZr_{0.1}Ce_{0.7}Y_{0.1}Yb_{0.1}O_{3-\delta}$ (BZCYYb) anode-supported H-SOFC (H-DASC) for on-cell $CO_2$ dry reforming of $CH_4$ (DRC). For demonstrating the effectiveness of LSCrN@Ni, a cell without adding LSCrN@Ni catalyst (H-CASC) is also studied comparatively. Fueled with $H_2$, both H-CASC and H-DASC show similar stable performance with a maximum power density ranging from 0.360 to 0.816 W $cm^{-2}$ at temperatures between 550 and 700 °C. When $CO_2$-$CH_4$ is used as fuel, the performance and stability of H-CASC decrease considerably with a maximum power density of 0.287 W $cm^{-2}$ at 700 °C and a sharp drop in cell voltage from initial 0.49 to 0.10 V within 20 h under 0.6 A $cm^{-2}$. In contrast, H-DASC demonstrates a maximum power density of 0.605 W $cm^{-2}$ and a stable cell voltage above 0.65 V for 65 h. That is attributed to highly efficient on-cell DRC by LSCrN@Ni.

## Introduction

Among all types of fuel cells, solid oxide fuel cells (SOFCs) show some compelling advantages, such as high efficiency and fuel flexibility.[1-3] Conventional SOFCs use an oxygen ion-conducting electrolyte like yttria-stabilized zirconia (YSZ) and Gd-doped cerium oxide (GDC) and are operated usually at temperatures above 700 °C, and stringent requirements on materials and maintenance are necessary.[4-7] Recently, SOFCs with a proton-conducting electrolyte (H-SOFCs) have attracted increasing attention due to their lower operation temperatures (500–700 °C)[8-12] and theoretically higher efficiency as $H_2O$ produced in the cathode without diluting the fuel in the anode.[13-15]

However, H-SOFCs are facing a challenge that hydrocarbons cannot be used directly as no oxygen ions available in the anode of H-SOFCs operated at relatively low temperatures or under high steam partial pressure ($pH_2O$) to oxidize the carbonaceous species. To circumvent this difficulty, reforming of hydrocarbons, by either steam or $CO_2$[16-19], is often considered to produce $H_2$ and CO. Then $H_2$ can be used as the fuel for H-SOFCs for power generation, and CO can be collected at the anode exhaust as a valuable chemical product that can be used for the industries of organic synthesis and metallurgical engineering. $CH_4$ is a primary constituent of natural gas, coal gas and biogas, and is also a greenhouse gas like $CO_2$. Thus, $CO_2$ reforming of $CH_4$ called dry reforming of $CH_4$ (DRC) has drawn more and more attentions[20], as it takes advantage of abundantly available resources and converts two greenhouse gases into fuel for power generation by H-SOFCs[21, 22] and a high-value product for chemical engineering. The heat released by the exothermic reactions in the anode and cathode of H-SOFCs can be used for the endothermic DRC reaction to enable a thermally autogenous process[23]. To save an external reformer for a simplified and low-cost H-SOFC power generation system, and increasing the thermal efficiency, the DRC reaction is better to occur in the anode[24-26].

So far, the state-of-the-art anode material is Ni-cermet consisting of Ni and an electrolyte material, which is not an active DRC catalyst[13, 27], and is also suffered from carbon deposition. In addition, the most widely used proton-conducting electrolyte, doped $BaCeO_3$, is not chemically stable in $CO_2$-containing atmospheres[28-31], which presents another challenge to DRC occurring in the anode.

To overcome these challenges, an additional layer of catalyst for DRC was positioned on the surface of the Ni-cermet anode of an anode-supported cell in the present study. The function of the DRC catalyst is to on-cell reform $CH_4$ by $CO_2$, producing a CO and $H_2$ rich syngas and avoiding an excessive amount of $CH_4$ and $CO_2$ to reach into the anode. And the $H_2$ was electrochemically oxidized by the anode for power generation and the CO was collected at the anode exhaust as a valuable chemical product, as shown in Fig. 1. The material of the DRC catalyst used was A-site deficient perovskite $La_{0.6}Sr_{0.2}Cr_{0.85}Ni_{0.15}O_{3-\delta}$ (LSCrN), which has demonstrated high

a Center for Fuel Cell Innovation, School of Materials Science and Engineering, State Key Lab of Material Processing and Die & Mould Technology, Huazhong University of Science and Technology, Wuhan, 430074, China.
* E-mail: jialc@hust.edu.cn
b Department of Mechanical Engineering, University of South Carolina, Columbia, SC, 29208, United States.
* E-mail: chenfa@cec.sc.edu
c School of Physics and Information Engineering, The Key Laboratory of Optoelectronic Chemical Materials and Devices, Jianghan University, Wuhan 430056, China.
‡ These authors contributed equally.

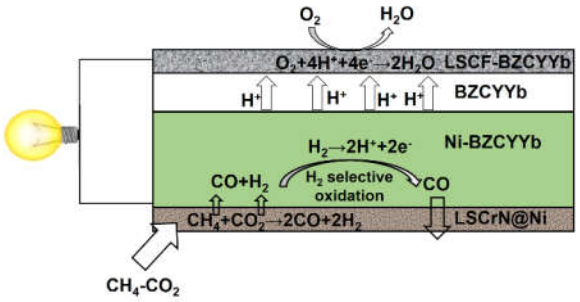


Fig. 1 Schematic diagram of on-cell $CO_2$ dry reforming of $CH_4$ in an anode supported SOFC cell.

catalytic activity for DRC and remained stable in the anode atmosphere[32]. In this paper, the electrochemical performance and stability of the cells with and without LSCrN catalyst are reported to demonstrate the effectiveness of LSCrN on the direct use of $CO_2$ and $CH_4$ in H-SOFCs for power generation and CO production, without carbon deposition in the Ni-cermet anode and $CO_2$-poisoning of the $BaCeO_3$ based electrolyte.

## Results and discussion

### Materials characteristics and compatibility/stability

Fig. 2 shows the XRD results of various specimens prepared above. As-prepared LSCrN and BZCYYb were a single-phase material in perovskite structure like that of $LaCrO_3$ and $BaCeO_3$, respectively. And they were chemically compatible both in the air at 1100 °C and in $H_2$ at 800 °C, indicated by that no additional phases were formed in the heat-treated mixtures, except a metallic Ni phase in the reduced LSCrN. This chemical compatibility would assure that there was no additional phase formation during LSCrN-BZCYYb catalyst was added on the anode at temperatures up to 1100 °C, and H-DASC was operated at temperatures between 550 and 700 °C. The LSCrN reduced in pure $H_2$ for 4 h at 800 °C consisted of a primary phase of perovskite LSCrN and a secondary phase of metallic Ni, indicating that Ni exsolution from LSCrN occurred during the reduction (Fig. 2a). According to the results of the Rietveld refinement using Pbnm space symmetry for LSCrN perovskite and Fm3m space symmetry for Ni (Fig. S1, Table S1), the ratio of perovskite to metallic Ni was 0.878/0.122 and approximately 81% of the Ni in LSCrN originally exsolved from the perovskite structure, following the reaction:

$$La_{0.6}Sr_{0.2}Cr_{0.85}Ni_{0.15}O_3 + 0.122\ H_2 \rightarrow 0.878\ La_{0.683}Sr_{0.228}Cr_{0.968}Ni_{0.032}O_{3-\delta} + 0.122\ Ni + 0.122\ H_2O \quad (1)$$

And the exsolution process was completed almost within 3 h at 800 °C in 5% $H_2$-Ar atmosphere, indicated by thermogravimetric analysis (Fig. S2).

BZCYYb decomposed partially and completely into $BaCO_3$ and $CeO_2$ in $CH_4$-$CO_2$ and pure $CO_2$ atmospheres for 6 h at 700 °C, respectively, indicating that $CO_2$ is the component that caused the decomposition, while remained stable in CO-$H_2$ atmosphere (Fig 2b). It is also noticed that the BZCYYb disc broke and surface morphology changed with small granules of $BaCO_3$ after being treated in pure $CO_2$ at 700 °C for 20 h (Fig. S3). Based on the stability results above, it is reasonable to expect that the anode and the electrolyte of the cells would be disintegrated in $CO_2$-containing atmospheres with time, and the on-cell DRC with LSCrN catalyst is necessary to avoid their exposure to $CO_2$ and ensure the cell performance.

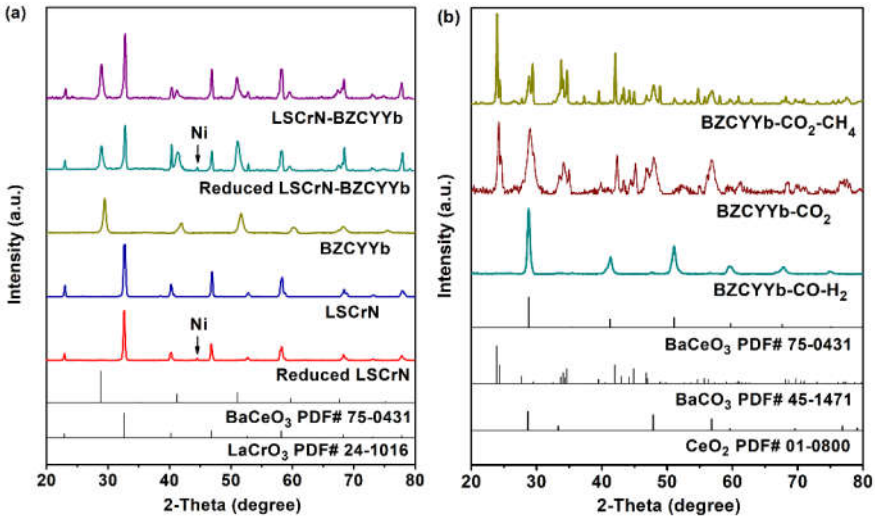


Fig 2. X-ray diffraction patterns of various prepared and treated materials: (a) as-prepared BZCYYb and LSCrN, reduced LSCrN in $H_2$ at 800 °C for 4 h, and LSCrN-BZCYYb mixture calcined at 1100 °C in the air for 3 h and that reduced in $H_2$ at 800 °C for 3 h; (b) BZCYYb heat-treated in $CH_4$-$CO_2$, CO-$H_2$ and pure $CO_2$ flow at 700 °C for 6 h.

**Cell and LSCrN@Ni microstructures**

Fig. 3 shows the cross-sectional microstructure of H-DASC reduced in $H_2$ at 800 C for 4 h. The cell was well sintered at the interfaces with a LSCF-BZCYYb cathode (~40 μm), a dense BZCYYb electrolyte (~10 μm), a porous Ni-BZCYYb anode (Fig. 3a), and a porous LSCrN@Ni DRC catalyst (~50 μm, Fig. 3b). After reduction, the Ni particles in the anode was submicron in size (Fig. 3c) and a part of the Ni in the LSCrN originally exsolved in situ in the form of uniformly distributed Ni nanoparticles supported on LSCrN substrate (Fig. 3d). The only difference in microstructure between reduced H-DASC and H-CASC was that there was not an LSCrN@Ni catalyst layer on the Ni-BZCYYb anode. Closely examined by TEM with a reduced LSCrN powder sample, the Ni exsolution was confirmed by the interplanar spacings of the Ni nanoparticle and the substrate, and the exsolved Ni nanoparticles were partially embedded in the LSCrN substrate (Fig. S4).

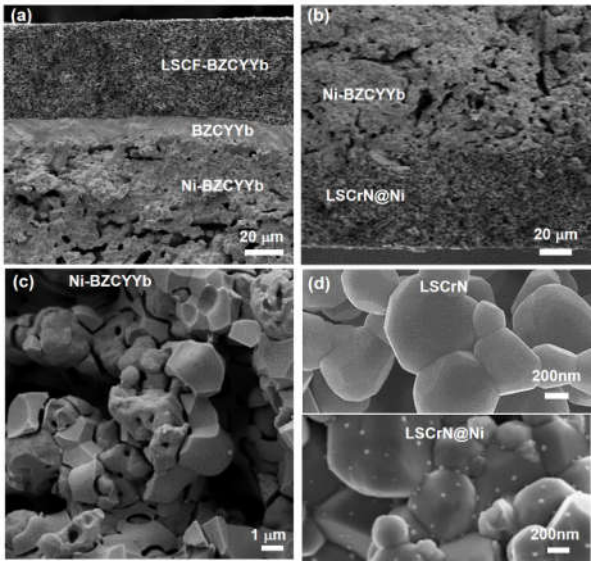


Fig. 3 Microstructure of H-DASC: (a) LSCF-BZCYYb cathode/BZCYYb electrolyte/Ni-BZCYYb anode; (b) LSCrN@Ni catalyst layer/Ni-BZCYYb anode; (c) Ni-BZCYYb anode; and (d) LSCrN DRC catalyst before and after reduction.

**Cell performances**

As a benchmark, both H-CASC and H-DASC were evaluated firstly with $H_2$ fuel, as shown in Fig. 4. They demonstrated similar high performance at temperatures between 550 and 700 °C with a maximum power density ranging from 0.360 to 0.816 W $cm^{-2}$ (Fig. 4a), a cell ohmic ($R_\Omega$)/polarization ($R_P$) resistance from 0.26/0.40 to 0.17/0.09 Ω $cm^2$ (Fig. 4b), and performed stably for 100 h at 700 °C under 1.0 A $cm^{-2}$ with a cell voltage of approximately 0.7 V (Fig. 4c). This similarity in performance of H-CASC and H-DASC indicates that the addition of a layer of LSCrN@Ni on the Ni-BZCYYb anode did adversely affect the intrinsic cell performance.

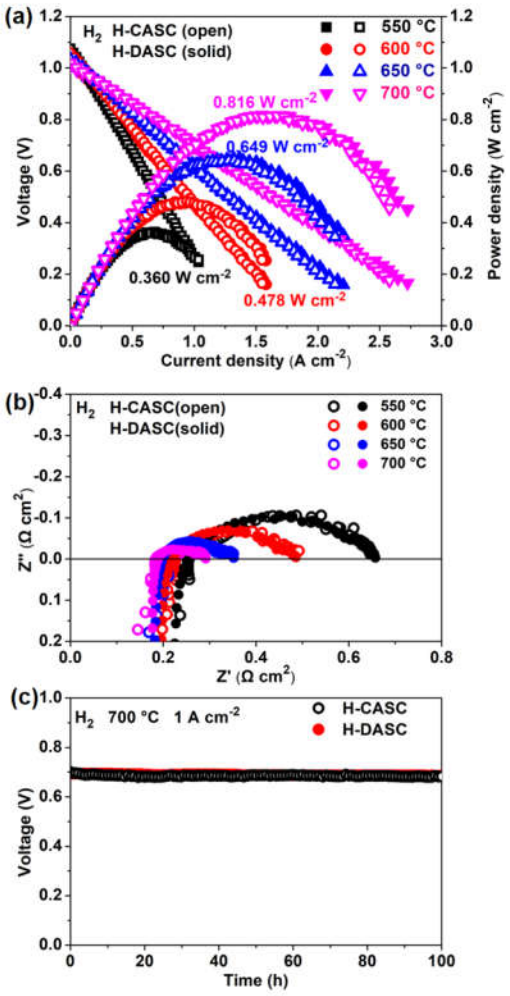


Fig. 4 Performance of H-CASC (open) and H-DASC (solid) with $H_2$ fuel at temperatures between 550 and 700 °C: (a) I-V-P curves, (b) open circuit impedance spectra, (c) performance stability at 700 °C and 1.0 A $cm^{-2}$.

To validate the effectiveness of LSCrN@Ni catalyst for on-cell DRC, both H-CASC and H-DASC were then evaluated with $CO_2$-$CH_4$ as fuel. Fig. 5 shows the performance, post-test examination, and anode exhaust composition of H-CASC. It is clearly seen that the performance was much lower than that with $H_2$ as fuel, the maximum power density was from 0.06 to 0.287 W cm$^{-2}$ at temperatures between 550 and 700 °C (Fig. 5a) with a high value of $R_P$ between 1.98 and 0.549 Ω cm$^2$ (Fig. 5b), in contrast to from 0.360 to 0.816 W cm$^{-2}$ and from 0.40 to 0.09 Ω cm$^2$, as shown above. Moreover, the cell voltage at 700 °C under 0.6 A cm$^{-2}$ decreased immediately with time from the initial 0.49 V to approximately at the level of 0.1within 20 h (Fig. 5c). And at the same time, more and more amounts of $CO_2$ and $CH_4$ existed in the anode exhaust (Fig. 5d), indicating that the reforming capability of the Ni-BZCYYb anode to form CO and $H_2$ was compromised gradually with time, even though the initial activity for reforming was not adequately high. One reason for the above degraded cell performance was the decomposition of BZCYYb in $CO_2$-$CH_4$ atmosphere by the reaction between BZCYYb and $CO_2$ to form $BaCO_3$ granules on the surface, as shown by Raman spectroscopy (Fig. 5e) and XRD (Fig. 2b) analyses and SEM examination (Fig. 5f). And the other was carbon deposition (foam-like carbon) in the anode that covered the active sites for reactions, as shown by Raman spectroscopy analysis (Fig. 5e) and SEM examination (Fig. 5f). The $BaCO_3$ granules on the BZCYYb and the deposited carbon surrounding the Ni particles in the Ni-BZCYYb anode would prevent the adsorption of $CO_2$ on BZCYYb and of $CH_4$ on Ni for the DRC reactions, consequently, the capability of the anode for DRC was gradually compromised with time.

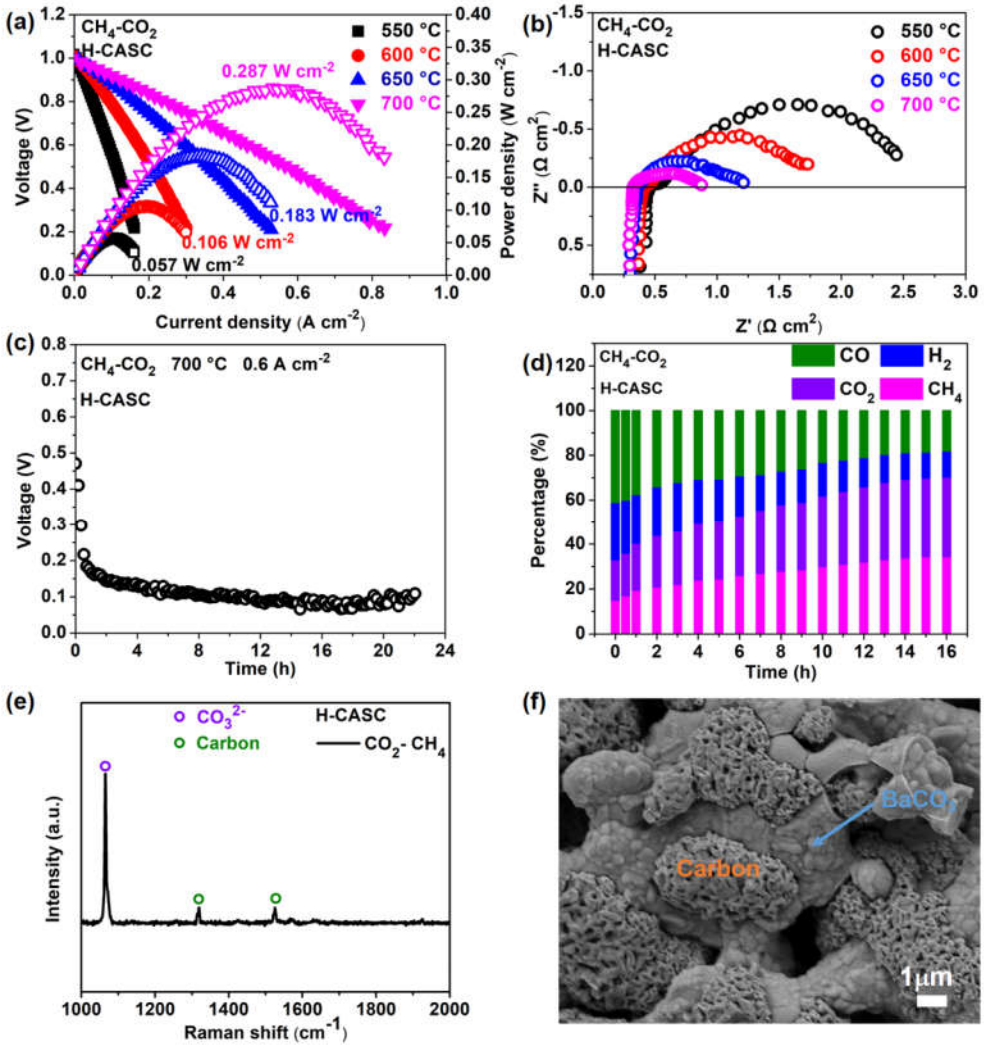


Fig. 5 Performance and characterization of H-CASC tested with $CO_2$-$CH_4$ fuel at temperatures between 550 and 700 °C: (a) I-V-P curves, (b) open circuit impedance spectra, (c) performance stability at 700 °C and 0.6 A cm$^{-2}$, (d) anode exhaust composition with time, (e) Raman spectra taken at anodes after stability test, and (f) anode microstructure after stability test.

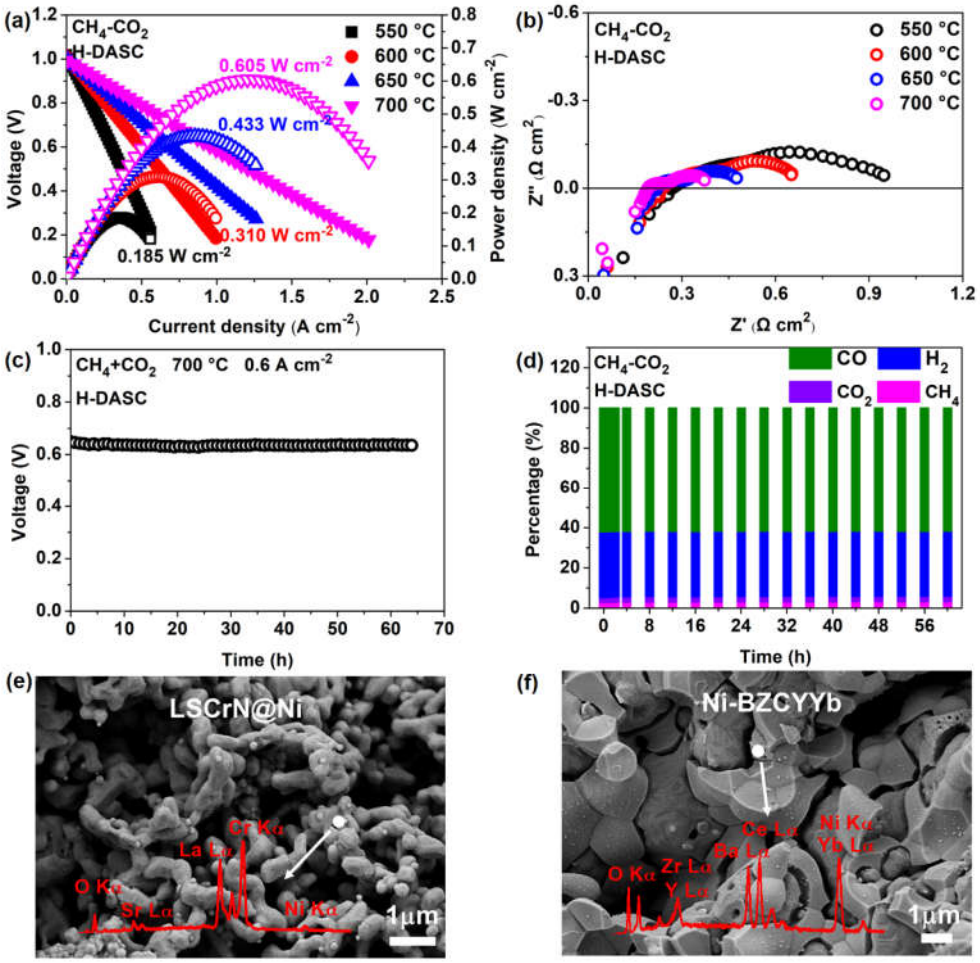


Fig. 6 Performance and characterization of H-DASC tested with $CO_2$-$CH_4$ fuel at temperatures between 550 and 700 °C: (a) I-V-P curves, (b) open circuit impedance spectra, (c) performance stability at 700 °C and 0.6 A $cm^{-2}$, (d) anode exhaust composition with time, (e) microstructure and EDS analysis of LSCrN@Ni after stability test, and (f) anode microstructure and EDS analysis after stability test.

Compared with H-CASC, H-DASC demonstrated a much-improved performance, as shown in Fig. 6. The maximum power density was significantly higher from 0.185 to 0.605 W $cm^{-2}$ at temperatures between 550 and 700 °C (Fig. 6a) with a smaller value of $R_P$ between 0.678 and 0.181 Ω $cm^2$ (Fig. 6b). And the cell operated for 65 h at 700 °C under 0.6 A $cm^{-2}$, approaching a stable voltage above 0.65 V (Fig. 6c). This high performance of H-DASC with $CO_2$-$CH_4$ as fuel is because of the following reasons. First, the catalytic activity of LSCrN@Ni for DRC reactions is considerably high and much higher than that of the Ni-BZCYYb anode. For example, almost all the $CO_2$ and $CH_4$ in the fuel were converted into CO and $H_2$ at 700 °C, and the activity remained unchanged essentially during the durability test for up to 65 h (Fig. 6d). Second, the catalyst LSCrN@Ni is resistant to carbon deposition due to the strong interaction between the exsolved Ni nanoparticles and the oxygen vacancy-abundant LSCrN substrate.[32] As noted, after 65 h operation at 700 °C under 0.6 A $cm^{-2}$, no deposited carbon was observed in the layer of LSCrN@Ni (Fig. 6e). And thirdly and most importantly, the Ni-BZCYYb anode was free of deposited carbon, and the BZCYYb in the anode remained stable essentially without forming observable $BaCO_3$ granules on its surface (Fig. 6f). The free of carbon deposition and observable $BaCO_3$ formation in LSCrN@Ni catalyst and Ni-BZCYYb anode was also supported by Raman analysis, as shown in Fig. S5. Therefore, the above results suggest that the $CO_2$ in the fuel was consumed completely in the layer of the DRC catalyst LSCrN@Ni for $CH_4$ reforming, and did not reach the Ni-BZCYYb anode, and only the reformate of CO and $H_2$ that is no harm on BZCYYb arrived in the anode.

## Experimental

### Materials preparation

For the use of the cathode and electrolyte, $BaZr_{0.1}Ce_{0.7}Y_{0.1}Yb_{0.1}O_{3-\delta}$ (BZCYYb) powder was synthesized by a sol-gel method. Firstly, $Ba(NO_3)_2$ (99.0 %, Alfa Aesar), $Zr(NO_3)_2$ solution (35 wt%, Sigma-Aldrich), $Ce(NO_3)_26H_2O$ (99.5 %, Alfa Aesar), $Y(NO_3)_36H_2O$ (99.9 %,

Alfa Aesar) and $Yb(NO_3)_3 5H_2O$ (99.9 %, Sigma-Aldrich) in proportional amount were dissolved in distilled water. Subsequently, ethylenediaminetetraacetic acid (EDTA, 99.4 %, Alfa Aesar) and citric acid monohydrate (CA, 99.5 %, Sigma-Aldrich) were added as the chelating agent and $NH_4OH$ (28-30 %, VWR Chemicals) for pH value adjustment. The molar ratio of total metal cations to EDTA to CA was 1:1:1.5, and the pH value of the solution to about 8. The solution was heated under agitation to form a transparent gel, which was combusted in a microwave oven and then calcined at 1100 °C in the air for 5 h to obtain BZCYYb powder. The same sol-gel method was also adopted for the synthesis of $La_{0.6}Sr_{0.4}Co_{0.2}Fe_{0.8}O_{3-\delta}$ (LSCF) powder for the cathode and $La_{0.6}Sr_{0.2}Cr_{0.85}Ni_{0.15}O_{3-\delta}$ (LSCrN) powder for the DRC catalyst. The calcination was conducted for LSCF and LSCrN at 900 and 1200 °C, respectively, in the air for 3 h. To understand Ni exsolution in LSCrN in reducing atmosphere, the prepared LSCrN was reduced in $H_2$ at 800 °C for 4 h to simulate the pre-reduction conditions of the cell for a complete reduction of NiO in the anode before the electrochemical test. For the anode that supports the cell needs a larger pore size for fuel gas transport; therefore, the BZCYYb powder used in the anode was prepared by a solid-reaction process, in which stoichiometric amounts of $BaCO_3$ (99.8 %, Alfa Aesar), $ZrO_2$ (99.7 %, Alfa Aesar), $CeO_2$ (99.9 %, Alfa Aesar), $Y_2O_3$ (99.9 %, Alfa Aesar) and $Yb_2O_3$ (99.9 %, Alfa Aesar) powders were mixed and ball-milled in ethyl alcohol for 12 h, and calcined at 1100 °C for 10 h. This process was repeated for several times until a single-phase perovskite BZCYYb powder was achieved.

**Single-cells fabrication**

The conventional proton-conducting anode-supported single-cell (H-CASC) consisted of NiO-BZCYYb anode, BZCYYb electrolyte, and LSCF-BZCYYb. The anode was made by ball-mixing commercial NiO (99 %, J.T. Baker), BZCYYb and powdery graphite (pore former) at a weight ratio of 9:6:5 in ethyl alcohol, followed by drying, die-pressing and pre-sintering at 1050 °C in air for 2 h. The BZCYYb electrolyte was made by coating BZCYYb slurry on the surface of the anode and then sintering at 1450 °C in the air for 5 h for densification of the BZCYYb electrolyte. The LSCF-BZCYYb cathode was made by printing LSCF-BZCYYb ink, which was composed of LSCF, BZCYYb, and a low viscosity vehicle (V-006A, Heraeus, US) at a weight ratio of 1:1:3, on the sintered electrolyte, followed by sintering at 1050 °C in the air for 2 h. Finally, the thickness of the anode was about 1 mm, and the cathode active area was 0.5 $cm^2$. For on-cell DRC, LSCrN ink comprising of LSCrN and V-006A at a weight ratio of 2:3 was printed on the anode and then calcined at 1100 °C in the air for 2 h before preparing the cathode. This cell, designated as H-DASC, had an on-cell reforming LSCrN layer of about 50 μm.

**Materials and cells characterization**

X-diffraction (XRD, 7000, Shimadzu) with a CuKα radiation and a D/teX silicon strip detector was employed for examining the phases and structures in as-prepared BZCYYb and LSCrN powders, the chemical compatibility between BZCYYb and LSCrN in air and reducing atmosphere, and the chemical stability of BZCYYb powder at 700 °C in $CH_4$-$CO_2$ (1:1 molar ratio), CO-$H_2$ (1:1 molar ratio) and pure $CO_2$ atmospheres. The sample for the compatibility examination was a mixture of BZCYYb and LSCrN at 1:1 weight ratio and heat-treated at 1100 °C in the air for 3 h or at 800 °C in pure $H_2$ for 3 h.

To understand the stability of sintered BZCYYb electrolyte in $CO_2$-containing atmosphere, a BZCYYb disc, prepared by die-pressing and sintering at 1500 °C in the air for 5 h, was treated at 700 °C in $CO_2$ flow for 5, 10 and 20 h, respectively, and examined by a field emission electron scanning microscope (FE-SEM, Gemini 300, Zeiss). A transmission electron microscope (TEM, FEI Titan ETEM G2 80-300) with an energy-dispersive X-ray spectrometer (EDS) was used for the examination of the reduced LSCrN. The microstructure of the cells before and after electrochemical tests was also examine by SEM/EDS. A Raman spectrometer (Horiba Xplora Plus) was utilized to analyze the effect of $CO_2$ on BZCYYb and carbon deposition in post-test cell, and thermogravimetric analysis (TG-DSC, Netzsch STA 449F3) was performed to understand the process of LSCrN reduction from room temperature to and at 800 °C at a rate of 10 °C $min^{-1}$ in 5%$H_2$-Ar atmosphere.

The electrochemical performance of the cells, including current density (I)-voltage (V)-powder density (P) curves and electrochemical impedance spectra (EIS), was evaluated by using an electrochemical station (VersaSTAT 3-400, Princeton Applied Research). Pt slurry was painted on the surface of the cathode and the anode as the current collector. Before the test, the cell was attached to an $Al_2O_3$ tube (cell holder) with a ceramic sealing material (Ceramabond, Aremco Products) and pre-reduced in situ by passing $H_2$ to the anode at 800 °C for 4 h to reduce LSCrN in the DRC catalyst and NiO in the anode. The reduced LSCrN was designated as LSCrN@Ni, as Ni exsolution occurred during reduction with Ni nanoparticles supported by LSCrN substrate. During the test at temperatures from 550 to 700 °C, wet $H_2$ (3% $H_2O$, 20 mL $min^{-1}$) was used as a benchmark, and $CH_4$-$CO_2$ (1:1 ratio, 10 mL $min^{-1}$) to demonstrate the effectiveness of LSCrN@Ni for on-cell DRC. In the performance stability test at 700 °C with $CH_4$-$CO_2$ fuel, the anode exhaust gas was carried by Ar to a gas chromatograph (Panna A91) equipped with a Porapak Q, a molecular sieve 5 A column and a TCD detector for composition analysis.

## Conclusions

In this study, anode-supported proton-conducting H-SOFC cells, with (H-DASC) and without (H-CASC) a layer of LSCrN@Ni catalyst on the Ni-BZCYYb anode for on-cell dry reforming of $CH_4$ by $CO_2$, were evaluated comparatively with $H_2$ and $CO_2$-$CH_4$ fuels, respectively. Based on the results obtained, the following conclusions are made.

1) BZCYYb is not stable in $CO_2$-containing atmospheres at 700 °C because of BZCYYb decomposition into $BaCO_3$ and $CeO_2$, presenting potential damage of integrity for the anode and electrolyte. And the degree of BZCYYb decomposition increases with increasing $CO_2$ composition, but it is stable in the CO-$H_2$ atmosphere.
2) With $H_2$ as fuel, the performance of H-CASC and H-DASC is similar to each other, and the addition of LSCrN@Ni on-cell DRC catalyst on the Ni-BZCYYb anode does not affect adversely on the intrinsic behavior of the cell.

3) Ni-BZCYYb is not an efficient catalyst for DRC reactions. Carbon deposition and BZCYYb decomposition in Ni-BZCYYb anode result in poor and short-term performance of H-CASC with $CH_4$-$CO_2$ as fuel. Foam-like deposited carbon and $BaCO_3$ granules cover the surface of Ni and BZCYYb, respectively, compromising the catalytic and electrochemical activities of the Ni-BZCYYb anode.
4) LSCrN@Ni is proved to be an active and coking-resistant catalyst for on-cell DRC reactions, converting almost all $CO_2$ and $CH_4$ into CO and $H_2$. H-DASC with $CH_4$-$CO_2$ as fuel demonstrates a significantly higher and much more stable performance than that of H-CASC, benefited from the on-cell DRC by LSCrN@Ni that produces high concentration $H_2$ in the reformate and prevents $CO_2$ and $CH_4$ reaching the anode for carbon deposition and BZCYYb decomposition.

## Conflicts of interest

There are no conflicts to declare.

## Acknowledgements

This research was financially supported by the National Key Research and Development Program of China (2018YFE0124700), the National Natural Science Foundation of China (U1910209, U1601207, 51872103) and the Hubei Province Natural Science Foundation (2018CFB172) and the U.S. National Science Foundation (DMR-1832809). The characterizations were assisted by the Analytical and Testing Center of Huazhong University of Science and Technology and the State Key Laboratory of Material Processing and Die/Mould Technology.

## Notes and references

1. R. M. Ormerod, *Chemical Society Reviews*, 2003, **32**, 17-28.
2. P. Singh and N. Q. Minh, *International Journal of Applied Ceramic Technology*, 2004, **1**, 5-15.
3. O. Yamamoto, *Electrochimica Acta*, 2000, **45**, 2423-2435.
4. Z. Gao, E. C. Miller and S. A. Barnett, *Advanced Functional Materials*, 2014, **24**, 5703-5709.
5. J. A. Dawson, J. A. Miller and I. Tanaka, *Chemistry of Materials*, 2015, **27**, 901-908.
6. S. Sun and Z. Cheng, *Journal of The Electrochemical Society*, 2017, **164**, F81-F88.
7. S. Sun and Z. Cheng, *Journal of The Electrochemical Society*, 2017, **164**, F3104-F3113.
8. Y. Xia, Z. Jin, H. Wang, Z. Gong, H. Lv, R. Peng, W. Liu and L. Bi, *Journal of Materials Chemistry A*, 2019, **7**, 16136-16148.
9. X. Xu, H. Wang, J. Ma, W. Liu, X. Wang, M. Fronzi and L. Bi, *Journal of Materials Chemistry A*, 2019, **7**, 18792-18798.
10. I.-H. Kim, D.-K. Lim, H. Bae, A. Bhardwaj, J.-Y. Park and S.-J. Song, *Journal of Materials Chemistry A*, 2019, **7**, 21321-21328.
11. L. Rioja-Monllor, C. Bernuy-Lopez, M.-L. Fontaine, T. Grande and M.-A. Einarsrud, *Journal of Materials Chemistry A*, 2019, **7**, 8609-8619.
12. S. Sun and Z. Cheng, *Journal of The Electrochemical Society*, 2018, **165**, F836-F844.
13. E. Fabbri, L. Bi, D. Pergolesi and E. Traversa, *Energy & Environmental Science*, 2011, **4**, 4984-4993.
14. E. Fabbri, L. Bi, D. Pergolesi and E. Traversa, *Advanced Materials*, 2012, **24**, 195-208.
15. S. Sun, O. Awadallah and Z. Cheng, *Journal of Power Sources*, 2018, **378**, 255-263.
16. C. Guerra, A. Lanzini, P. Leone, M. Santarelli and N. P. Brandon, *Journal of Power Sources*, 2014, **245**, 154-163.
17. B. Hua, M. Li, J.-l. Luo, J. Pu, B. Chi and J. Li, *Journal of Power Sources*, 2016, **303**, 340-346.
18. B. Hua, M. Li, J. Pu, B. Chi and L. Jian, *Journal of Materials Chemistry A,* 2014, **2**, 12576-12582.
19. S. E. Evans, J. Z. Staniforth, R. J. Darton and R. M. Ormerod, *Green Chemistry*, 2014, **16**, 4587-4594.
20. P. Tang, Q. Zhu, Z. Wu and D. Ma, *Energy & Environmental Science*, 2014, **7**, 2580-2591.
21. M. Li, B. Hua and J.-L. Luo, *ACS Energy Letters*, 2017, **2(8)**, 1789-1796.
22. W. Wang, C. Su, Y. Wu, R. Ran and Z. Shao, *Chemical Reviews,* 2013, **113**, 8104-8151.
23. K. T. Lee, C. M. Gore and E. D. Wachsman, *Journal of Materials Chemistry*, 2012, **22**, 22405-22408.
24. B. Hua, N. Yan, M. Li, Y.-q. Zhang, Y.-f. Sun, J. Li, T. Etsell, P. Sarkar, K. Chuang and J.-L. Luo, *Energy & Environmental Science*, 2016, **9**, 207-215.
25. Z. Zhan and S. A. Barnett, *Science*, 2005, **308**, 844-847.
26. C.W. Sun, Z. Xie, C.R. Xia, H. Li, L.Q. Chen, *Electrochem. Commun,* 2006, **8**, 833
27. B. Hua, N. Yan, M. Li, Y.-q. Zhang, Y.-f. Sun, J. Li, T. Etsell, P. Sarkar and J.-L. Luo. *Advanced Materials*, 2016, **28** (40),8921-8921.
28. T. Hibino, A. Hashimoto, M. Suzuki and M. Sano, *Journal of The Electrochemical Society*, 2002, **149**, A1503-A1508.
29. N. Zakowsky, S. Williamson and J. T. Irvine, *Solid State Ionics*, 2005, **176**, 3019-3026.
30. R. Kannan, K. Singh, S. Gill, T. Fürstenhaupt and V. Thangadurai, *Scientific Reports*, 2013, **3**, 2138.
31. S. Fang, K. S. Brinkman and F. Chen, *Journal of Membrane Science*, 2014, **467**, 85-92.
32. T. Wei, L. Jia, J. Luo, B. Chi, J. Pu and J. Li, *Applied Surface Science*, 2020, **506**, 144699.